ELSEVIER

Polymer 43 (2002) 2401–2408

polymer

www.elsevier.com/locate/polymer

Barrier properties of polypropylene/polyamide blends produced by microlayer coextrusion

D. Jarus, A. Hiltner*, E. Baer

Department of Macromolecular Science, Center for Applied Polymer Research, Case Western Reserve University, 10900 Euclid Ave., Cleveland, OH 44106-7202, USA

Received 7 September 2001; received in revised form 21 November 2001; accepted 26 November 2001

Abstract

The gas barrier properties of injection molded structures prepared from polymer microlayers were investigated. Polypropylene and polyamide-66 were combined as microlayers with tens to thousands of layers. A thin tie layer of compatibilizer coextruded between the layers provided adhesion. Injection molding the microlayered materials at a temperature intermediate between the melting points of the constituents resulted in a high volume fraction of high aspect ratio polyamide-66 microplatelets dispersed in a polypropylene matrix. The resulting material had significantly reduced permeability to oxygen and carbon dioxide compared to the conventional melt blend. Structural models for permeability indicated that enhanced barrier arose primarily from increased tortuosity of the diffusion pathway provided by the oriented, flat platelets of high aspect ratio in the skin region of the complex injected molded structure. © 2002 Published by Elsevier Science Ltd.

Keywords: Microlayer coextrusion; Nanolayer coextrusion; Polymer blends

1. Introduction

Blends of polypropylene (PP) with polyamide-66 (PA66) are attractive for barrier enhancement. The combination brings together the excellent gas barrier properties of a polyamide and the excellent water barrier typical of polyolefins. Unfortunately, homogeneous dispersion of the polyamide in the polyolefin matrix does not produce the desired barrier enhancement. Rather, the barrier properties follow those of the continuous matrix. A laminar morphology of the dispersed polyamide achieves good gas barrier by substantially increasing the tortuosity of the diffusion pathway [1]. Obtaining a dispersed phase of high aspect ratio by melt processing an immiscible polymer blend requires large biaxial extensional flows. Barrier properties close to those of the coextruded structure have been achieved with extrusion blow molding [2,3] or extrusion with special dies [4–6]. These approaches are limited to sheet or film. Achieving laminar blend morphologies by injection molding requires several blending steps [7], operating in a very narrow processing window [8], or using highly specialized feedblocks [9]. A compounding technique that induces a lamellar structure, which is subsequently retained during injection molding, is ideal.

Nanolayer and microlayer coextrusion is a method for combining two or three polymers as tens, hundreds or thousands of alternating layers with individual layers as thin as tens of nanometers [10,11]. Concepts for utilizing microlayer coextrusion as a blending tool for creating microplatelets of high aspect ratio were explored in a previous study [12]. Two polymers were combined as microlayers and subsequently processed at a temperature that melted one of the constituents while leaving the other dispersed as layers of high aspect ratio. Despite the large difference in melt viscosities, it was possible to combine PP and PA66 as microlayers with more than 2000 layers and nominal layer thicknesses as small as 0.5 μm. Retention of the PA66 layer structure during subsequent injection molding produced a high volume fraction of PA66 microplatelets dispersed in a PP matrix. The resulting material had excellent oxygen barrier properties. An enhancement of 4–5 times over the barrier of the conventional melt blend resulted from increased tortuosity of the diffusion pathway.

The promising gas barrier characteristics of injection molded microlayers of PP and PA66 reported previously are further characterized in this paper. Oxygen and carbon dioxide barrier of the complex three-dimensional structures are compared. Following the conventional approach, the

* Corresponding author. Tel.: +1-216-368-4186; fax: +1-216-368-6329.
E-mail address: pah6@po.cwry.edu (A. Hiltner).

0032-3861/02/$ - see front matter © 2002 Published by Elsevier Science Ltd.
PII: S0032-3861(01)00790-X

effect of morphology is assessed in terms of gas permeability, with the assumption that morphology affects primarily diffusivity by altering the tortuosity of the diffusion pathway. Determinations of gas diffusivity and solubility in polymer blends are not common [13–16]. In the present study, the time-dependent flux is also examined, and when possible the diffusivity is extracted.

2. Materials and methods

2.1. Materials

An injection molding grade polypropylene (Huntsman P4G4Z-011, MFI = 12) (PP) and an extrusion grade PA66 (Dupont Zytel 42) (PA66) were combined with a maleated PP (Uniroyal Polybond 3150, 0.5 wt% maleic anhydride) (gPP) as microlayers and melt blends as described previously [12]. The volume ratio of PP/PA66/gPP was 65/25/10.

Microlayers with 33, 257 and 2049 layers were diced and injection molded at 180 °C, in between the melting points of PP and PA66, and at 280 °C, above the melting point of PA66. The melt blend was compression molded. For comparison, PA66 alone was either extruded or compression molded. The PP alone was injection molded.

Thin sections approximately 1 μm thick were microtomed from the coextruded microlayers for optical microscopy. Similarly, thin sections were microtomed from the injection molded plaques.

Oxygen flux at 25 °C, 0% relative humidity, and 1 atm pressure was measured with a MOCON OX-TRAN 2/20. Carbon dioxide flux at 25 °C, 0% relative humidity, and 1 atm pressure was measured with a MOCON PERMATRAN-C 4/40. Procedures for specimen conditioning, testing and data analysis were described previously [17]. Duplicate specimens were tested.

3. Results and discussion

3.1. Blend characterization

A longitudinal section of the coextruded microlayer with 257 layers is shown in Fig. 1(a). The microlayer consisted of 64 PA66 layers and 65 PP layers separated by thin tie layers of gPP with the overall composition 65/10/25 (PP/gPP/PA66). Due to their miscibility, PP and gPP layers were indistinguishable in optical micrographs; therefore the three-layer sequence gPP/PP/gPP appeared as a single layer separating the PA66 layers. The microlayer produced a series arrangement of the phases, albeit with a broad distribution in layer thickness due to the large viscosity mismatch between PP and PA66.

The 100 °C difference in the melting temperatures of PP and PA66 provided a broad window for injection molding the microlayers within which the PP layers melted to form

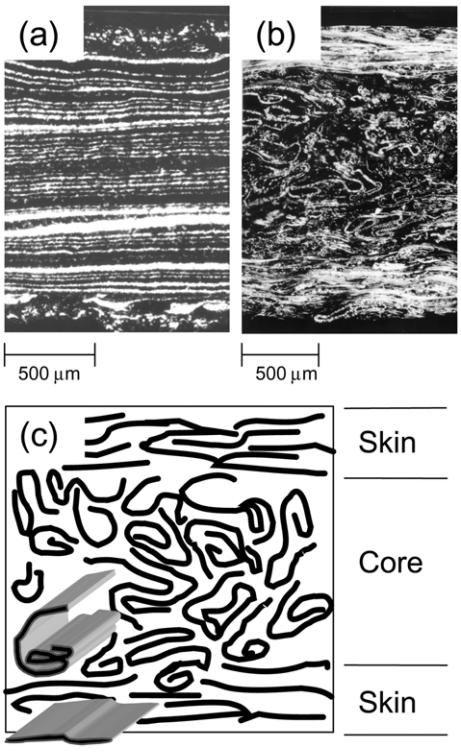

Fig. 1. Blend morphology: (a) microlayer with 257 layers; (b) 257 layers injection molded; (c) schematic representation of injection molded microlayer.

the matrix whereas the PA66 layers remained in the solid state as dispersed microplatelets of high aspect ratio. Injection molding the microlayer at 180 °C produced the complex morphology shown by the longitudinal cross-section in Fig. 1(b), and described in detail previously [12]. Due to the high aspect ratio of the flexible PA66 microplatelets, considerable curvature was induced by the shear fields encountered during injection molding. Flat platelets occurred only where the melt experienced elongational flow in the skin region of the injection molded skin–core structure.

The three dimensional schematic of the morphology in Fig. 1(c) shows the anisotropic skin–core structure with PA66 layers dispersed in the PP matrix. In the skin, the PA66 layers were largely oriented parallel to the surface. In the core, the PA66 layers were curled into cylinders that were oriented perpendicular to the injection direction. A previous study described the origin of the highly anisotropic morphology in the complex flow fields of the injection molding process [12].

For comparison, an isotropic 65/10/25 (PP/gPP/PA66) blend was prepared by conventional melt extrusion and subsequent compression molding. The blend morphology consisted of spherical PA66 particles dispersed in the continuous PP matrix. This morphology was also representative of the microlayer that was injection molded at a temperature high enough to melt the PA66 phase. Although the PA66 domains were slightly elongated in the skin, they

Table 1
Melting enthalpy and density of polypropylene, polyamide-66 and their blends

Material	Melting enthalpy (J g^{-1})				Density (g cm^{-3})
	First heating		Second heating		
	PP	PA66	PP	PA66	
PP	104 ± 2		104 ± 2		0.909 ± 0.001
PA66 as-extruded		64 ± 1		71 ± 1	1.126 ± 0.001
PA66 extruded and annealed at 240 °C		72 ± 1		71 ± 1	1.139 ± 0.002
PA66 compression molded at 280 °C		75 ± 1		72 ± 2	1.150 ± 0.001
33 layers as-extruded	78 ± 5	16 ± 1	76 ± 5	18 ± 1	0.957 ± 0.003
33 layers injection molded at 180 °C	78 ± 2	18 ± 2	76 ± 2	17 ± 2	0.964 ± 0.002
257 layers injection molded at 180 °C	77 ± 4	18 ± 2	76 ± 1	15 ± 1	0.961 ± 0.002
2049 layers injection molded at 180 °C	77 ± 1	18 ± 1	76 ± 1	16 ± 1	0.960 ± 0.002
257 layers injection molded at 280 °C	72 ± 2	17 ± 1	75 ± 2	16 ± 1	0.964 ± 0.001
Melt blend compression molded at 280 °C	75 ± 1	17 ± 1	80 ± 2	17 ± 1	0.966 ± 0.001

exhibited predominantly the spherical shape found in the conventional blend.

Melting enthalpy of the PP phase did not depend on the process history and was proportional to the melting enthalpy of PP based on blend composition (Table 1). There was no measurable effect of process history on the melting enthalpy of the PA66 phase, either. Because PA66 was the minor constituent of the blends, changes in crystallinity might not have been detected by thermal analysis.

The effect of thermal history on crystallinity of PA66 was demonstrated by exposing PA66 to the same process histories as experienced by the blends. Extrusion of PA66 under the conditions used to prepare the microlayers produced the lowest crystallinity as determined from either melting enthalpy or density (Table 1). Annealing extruded PA66 at the injection molding temperature increased the crystallinity. Compression molding produced the highest crystallinity of PA66. The blends followed the same trend in the density, which was a more sensitive measure of crystallinity than melting enthalpy. Thus, the coextruded microlayer had the lowest density and, by inference, the lowest crystallinity of the PA66 phase. Although PA66 did not melt during injection molding, the higher density of the injection molded microlayers, compared to the as-extruded microlayer, was attributable to annealing of the PA66 phase at the elevated temperature of injection molding. Compression molding produced the blend with the highest density and hence the highest PA66 crystallinity.

3.2. Barrier properties of polypropylene and polyamide-66

Careful specimen conditioning made it possible to obtain the initial, non-steady state gas flux. This part of the flux curve was determined mainly by the diffusivity D. As the permeant concentration reached a constant distribution, the flux reached the steady state value that reflected the permeability P. The time dependent flux $J(t)$ of a permeant gas at pressure p through a film of thickness l was fit to the solution of Fick's second law

$$J(t) = \frac{Pp}{l}\left[1 + 2\sum_{n=1}^{\infty}(-1)^n \exp\left(-\frac{D\pi^2 n^2 t}{l^2}\right)\right] \quad (1)$$

as described previously [17]. The excellent fit of the experimental oxygen flux illustrated in Figs. 2 and 3 resulted in extraction of D and an accurate determination of P. The solubility S was calculated as $S = P/D$. The carbon dioxide flux was similarly fit, however the larger error associated with carbon dioxide measurements resulted in greater uncertainty compared to the oxygen results (Table 2).

Permeability of PA66 to the gases studied was approximately two orders of magnitude lower than the permeability of PP (Table 2). This was due almost entirely to differences

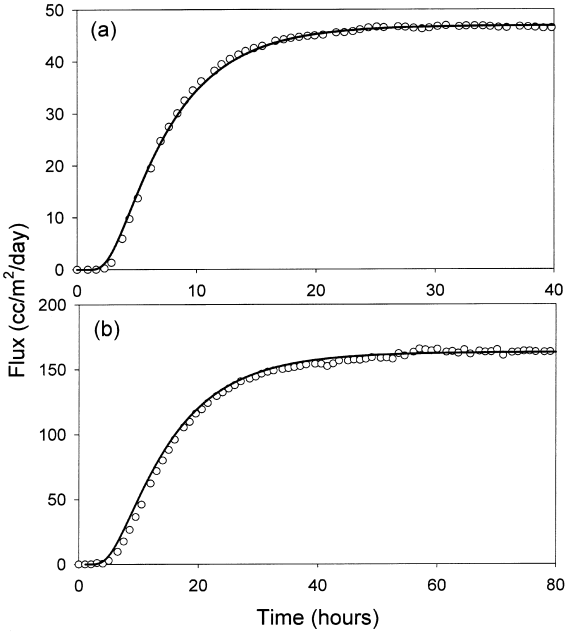

Fig. 2. Flux of permeant gases through injection molded PP: (a) oxygen; and (b) carbon dioxide.

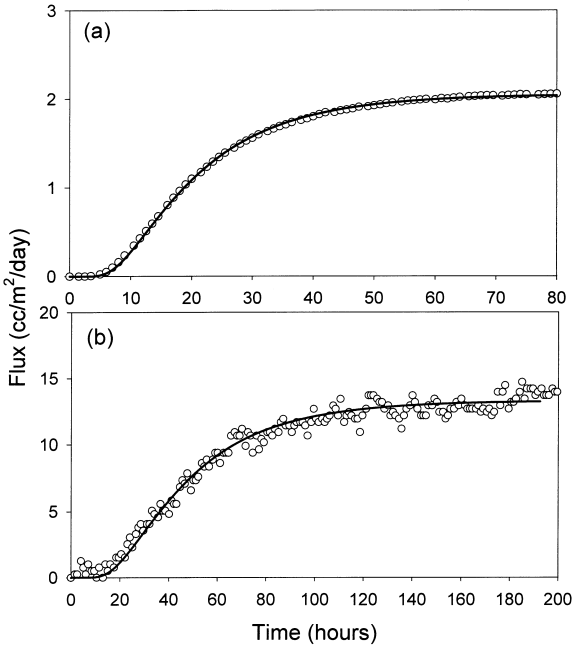

Fig. 3. Flux of penetrant gases through compression molded PA66: (a) oxygen; and (b) carbon dioxide.

in *D*. Compared to *D*, differences between PA66 and PP in *S* of the gases studied were negligible. In both PA66 and PP, *P* for carbon dioxide consistently exceeded *P* for oxygen by a factor of approximately four times. Although *D* for carbon dioxide was actually lower than *D* for oxygen, much higher *S* for carbon dioxide was responsible for the higher permeability.

Comparison of the various PA66 samples indicated that the gas transport parameters were affected by thermal and process history. Extruded PA66, with the lowest crystallinity, had the highest permeability. Annealing the extruded PA66 to increase the crystallinity reduced the permeability significantly. However, compression molded PA66, with the highest crystallinity, was almost as permeable to oxygen as extruded PA66. This was attributed to residual orientation in extruded PA66 that resulted from rapid quenching. Apparently the orientation was not completely lost during annealing because annealed PA66 had the lowest permeability of all the PA66 samples. The effects of thermal history on oxygen permeability of PA66 were qualitatively reproduced with carbon dioxide as the permeant.

3.3. Barrier properties of the blends

The flux curve of multiphase materials is amenable to analysis if only the continuous phase is permeable. The impermeable phase could be inert filler particles or the crystalline regions of a semicrystalline polymer [17,18]. Under these circumstances, the non-steady state Fickian solution can be used to extract *P*, *D* and subsequently *S* in the same way as for homogeneous materials with consideration given to the volume fraction and shape of the impermeable phase. The situation is much more complex if both phases are permeable, as with blends of immiscible polymers. Indeed, few studies of polymer blends attempt to characterize barrier properties other than permeability.

Unlike the well-known time lag method, the validity of the Fickian assumption could be tested with the flux data by the quality of the fit to Eq. (1). The compression molded blend, with uniform dispersion of spherical PA66 domains, fit Eq. (1) well in both non-steady state and steady state regions (Fig. 4(a)). The corresponding values of *P*, *D* and *S* are given in Table 3. Unlike *P* and *D*, which depend on blend morphology, *S* should depend only on blend composition and, at equilibrium, should equal the additive contributions of the blend constituents. Using compression molded PA66 as representative of the dispersed phase, and assuming gPP to have the same gas solubility as PP, *S* of the blend was calculated to be 0.054 $cm^3(STP)\ cm^{-1}\ atm^{-1}$, in excellent agreement with the value obtained from the fit values of *P* and *D*. Based on good fit to Eq. (1), and conformity of the resulting *S* with the additivity calculation, *D* and *P* values extracted from the Fickian analysis were understood to represent physical properties of the blend. The continuous PP phase clearly dominated the barrier properties of the melt blend. The presence of the less permeable PA66 phase decreased the permeability from 7.5 to 4.4 $cm^3(STP)\ cm\ m^{-2}\ atm^{-1}\ day^{-1}$ due to a reduction in diffusivity from 1.45 to $0.95 \times 10^{-11}\ m^2\ s^{-1}$.

The microlayer that had been injection molded at 280 °C, above the melting point of PA66, closely resembled the compression molded blend morphologically. It consisted primarily of spherical PA66 domains dispersed in the PP

Table 2
Transport parameters for polypropylene and polyamide-66 (*P*-permeability ($cm^3(STP)\ cm\ m^{-2}\ day^{-1}\ atm^{-1}$); *D*-diffusivity ($10^{-11}\ m^2\ s^{-1}$); *S*-solubility ($cm^3(STP)\ cm^{-3}\ atm^{-1}$))

Material	Oxygen			Carbon dioxide		
	P	*D*	*S*	*P*	*D*	*S*
PP injection molded at 180 °C	7.5 ± 0.1	1.45 ± 0.02	0.060 ± 0.001	26 ± 2	0.70 ± 0.01	0.42 ± 0.03
PA66 as-extruded	0.068 ± 0.005	0.016 ± 0.002	0.048 ± 0.002	0.28 ± 0.02	0.0018 ± 0.0002	1.79 ± 0.03
PA66 extruded and annealed at 240 °C	0.058 ± 0.002	0.019 ± 0.001	0.035 ± 0.002	0.18 ± 0.03	0.0020 ± 0.0001	1.03 ± 0.04
PA66 compression molded at 280 °C	0.064 ± 0.003	0.020 ± 0.002	0.037 ± 0.002	0.24 ± 0.01	0.0028 ± 0.0001	0.99 ± 0.01

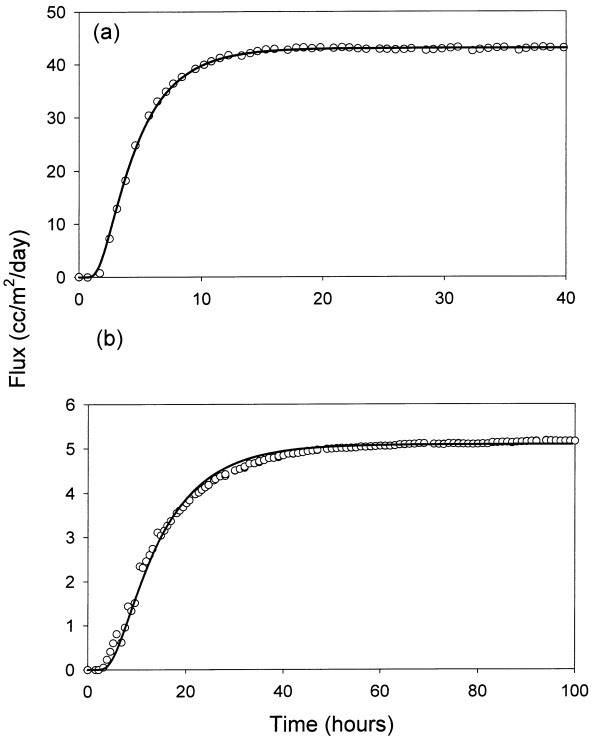

Fig. 4. Oxygen flux through: (a) compression molded melt blend; and (b) microlayer with 33 layers.

matrix with only a thin skin region containing elongated, cylindrical PA66 domains. Oxygen flux through this sample also gave an excellent fit with Eq. (1), and S calculated from the extracted values of P and D conformed to the additivity prediction (Table 3). Values of D and P also were similar to those of the compression molded sample, the slightly lower diffusivity, 0.87×10^{-11} compared to 0.95×10^{-11} m^2 s^{-1}, was attributed to an additional tortuosity effect imposed by the elongated PA66 domains in the skin.

The Fickian solution did not describe the initial non-steady state region of the oxygen flux curve for the coextruded microlayer as indicated by the poor fit of the solid curve to the data in Fig. 4(b). Furthermore, the flux did not reach a constant value at longer times, but continued to increase gradually. The values of P and D used to obtain the solid curve in Fig. 4(b) are included in Table 3. The low value of the resulting S, 0.037 compared to the additivity value of 0.054 cm^3(STP) cm^{-3} atm^{-1}, was further evidence that Eq. (1) did not apply.

Even if the non-steady state flux did not conform with the Fickian solution, the permeability could be obtained directly from the steady state flux F_0, the pressure gradient Δp, and the film thickness l as $P = F_0 l(\Delta p)^{-1}$. In this case, P was only an estimate because the flux did not reach a constant value on the time scale of the experiment. Achieving continuity of the higher barrier PA66 phase produced an order of magnitude decrease in the oxygen permeability from 4.4 for the compression molded blend to approximately 0.30 cm^3(STP) cm m^{-2} atm^{-1} day^{-1} for the microlayer.

The initial non-steady state portion of the oxygen flux curve for the injection molded microlayers conformed well with the Fickian solution. The solid lines in Fig. 5 were obtained from Eq. (1) with P and D values given in Table 3. Although the fit of the initial region was fairly good, the flux did not reach a constant steady state value. Small oscillations of the flux in the plateau region were evident for all the injection molded microlayers, and were particularly noticeable when the data were compared with the solid line solution to Eq. (1). This might have been caused by drift in the instrument over the long time period of the experiment.

Permeability of injection molded microlayers, estimated from the plateau flux, was intermediate between the melt blend and the microlayer. It appeared that blend morphology affected permeability primarily through D by altering the diffusion pathway through the continuous PP phase. In this regard, the oriented PA66 layers in the skin of the injection molded microlayer were more effective at increasing the tortuosity of the diffusion pathway than the curled layers in the core. Injection molding microlayers with more, thinner layers should have resulted in PA66 skin layers of higher aspect ratio, however the effect of layer thickness was subtle. The slightly lower P of injection molded microlayers with 257 layers compared to 33 layers may have reflected the higher aspect ratio of the skin layers. However, apparently increasing the aspect ratio further with 2049 layers either did not significantly change P (oxygen) or actually increased P (carbon dioxide). Various factors could

Table 3
Transport parameters for blends (P-permeability (cm^3(STP) cm m^{-2} day^{-1} atm^{-1}); D-diffusivity (10^{-11} m^2 s^{-1}); S-solubility (cm^3(STP) cm^{-3} atm^{-1}))

Material	Oxygen			Carbon dioxide		
	P	D	S	P	D	S
33 layers as-extruded	0.30 ± 0.03	0.095 ± 0.007	0.037 ± 0.001	1.11 ± 0.02	0.0083 ± 0.0003	1.5 ± 0.1
33 layers injection molded at 180 °C	1.08 ± 0.08	0.27 ± 0.03	0.047 ± 0.003	3.8 ± 0.2	0.099 ± 0.002	0.45 ± 0.02
257 layers injection molded at 180 °C	0.96 ± 0.03	0.22 ± 0.01	0.050 ± 0.001	3.0 ± 0.1	0.073 ± 0.001	0.47 ± 0.01
2049 layers injection molded at 180 °C	0.99 ± 0.02	0.23 ± 0.01	0.051 ± 0.001	3.6 ± 0.1	0.085 ± 0.003	0.49 ± 0.03
257 layers injection molded at 280 °C	4.0 ± 0.1	0.87 ± 0.01	0.053 ± 0.001			
Melt blend compression molded at 280 °C	4.4 ± 0.1	0.95 ± 0.06	0.054 ± 0.003	15 ± 1	0.38 ± 0.01	0.46 ± 0.02

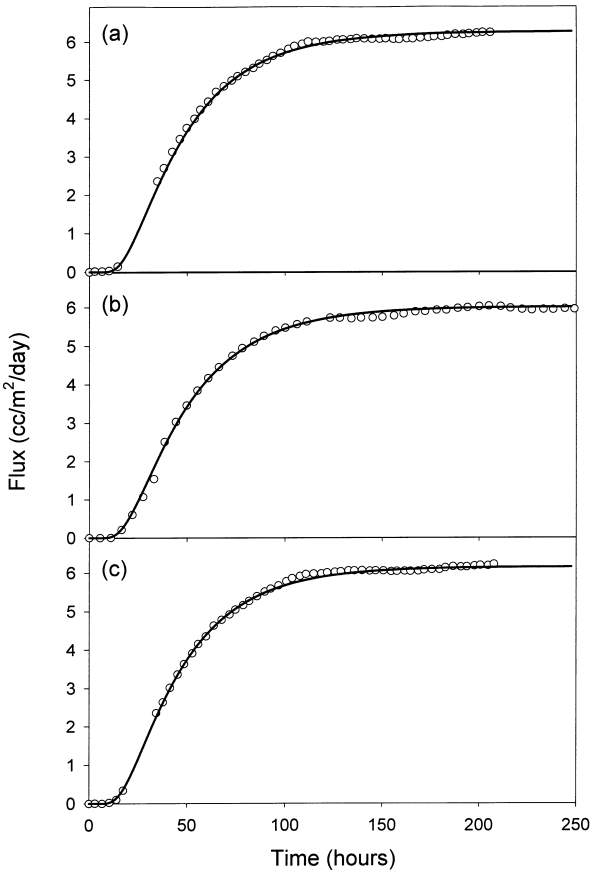

Fig. 5. Oxygen flux through injection molded microlayers: (a) 33 layers; (b) 7257 layers; and (c) 2049 layers.

explain this: aggregation of the very thin PA66 layers, breakup of layers either during coextrusion or subsequent injection molding, or higher diffusivity of very thin PA66 layers especially if the thickness was less than the spherulite size.

3.4. Models for permeability

Blend permeability was compared to predictions of the generalized Maxwell model for gas transport in heterogeneous media [19]. This model describes the compositional dependence of permeability in systems with a discontinuous low-permeability phase dispersed in a high-permeability matrix. The permeability P is given as

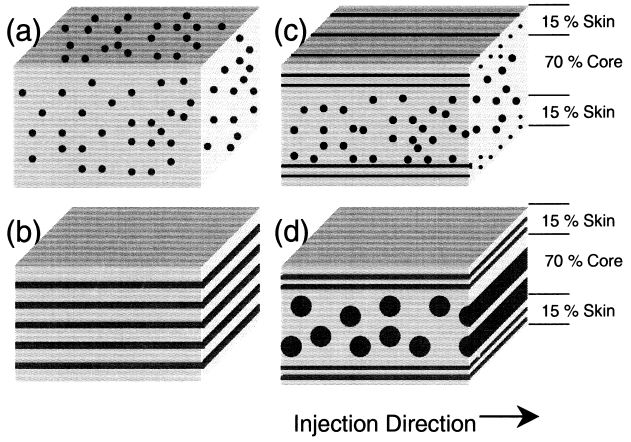

Fig. 6. Schematic representation of blend morphology for permeation models.

$$P = P_c\left[1 + \frac{(1+G)\phi_d}{\left(\frac{(P_d/P_c)+G}{(P_d/P_c)-1}\right) - \phi_d}\right] \quad (2)$$

where P_d is the permeability of the dispersed phase, P_c is the permeability of the continuous phase, and ϕ_d is the volume fraction of the dispersed phase. In this expression, G is a geometric factor that accounts for the shape of the dispersed phase. For a spherical dispersion, G is equal to 2; for a dispersion of long cylinders oriented perpendicular to the diffusional flow, G is equal to unity. For laminates, G is equal to zero if the layers are parallel to the flow, and infinity if the layers are perpendicular. These constitute lower and upper bounds, respectively, on the permeability.

The calculation was performed for the structures that were uniform through the thickness and without skin–core characteristics, specifically the compression molded melt blend, with dispersed spherical particles (Fig. 6(a)) and the microlayer of the same composition, with continuous layers of both constituents (Fig. 6(b)). To predict the permeability of these materials, gPP was assumed to have the same permeability as PP and possible interfacial effects of the graft copolymer were neglected. The value of P_d used in

Table 4
Comparison of measured permeability with composite models

Material PP/gPP/PA66 (65/10/25)	Oxygen permeability (cm^3(STP) cm m^{-2} atm^{-1} day^{-1})		Carbon dioxide permeability (cm^3(STP) cm m^{-2} atm^{-1} day^{-1})	
	Measured	Predicted	Measured	Predicted
33 layers coextruded	0.30	0.25 ($G = 0$) 0.26 (series)	1.1	1.0 ($G = 0$) 1.1 (series)
Melt blend	4.5	5.0 ($G = 2$)	15	17 ($G = 2$)
33 layers injection molded	1.08	0.67	3.8	2.2
257 layers injection molded	0.96	0.67	3.0	2.2
2049 layers injection molded	0.99	0.67	3.6	2.2
257 layers injection molded at 280 °C	4.0	4.9		

Eq. (2) was for the PA66 that most closely matched the thermal history. For the compression molded melt blend, this was compression molded PA66; for the microlayer, it was the as-extruded PA66. The morphology-based model satisfactorily described the permeability (Table 4), which entailed an order of magnitude difference between the contrasting structures.

For comparison, the calculation of the microlayer permeability based on a simple series arrangement of the constituents is included in Table 4

$$P = \left(\frac{\phi_d}{P_d} + \frac{\phi_c}{P_c} \right)^{-1} \quad (3)$$

where the symbols have the same meaning as in Eq. (2). Layer breakup at the surface of the coextruded microlayers can account for the small difference between the observed and predicted permeabilities.

Injection molded blends, with permeability intermediate between the melt blend and the microlayer, could have been described by Eq. (2) using an effective G value between zero and unity. However, changes in shape of the dispersed phase through the thickness that constituted the skin–core morphology ensured that the extracted G would not relate in a straightforward way to blend morphology. Instead, the skin–core morphology of injection molded blends was modeled as a three-layer composite consisting of a core layer and two identical skin layers (Fig. 6(c) and (d)). The layer permeabilities P_{skin} and P_{core} were modeled separately and combined in series as

$$P = \left(\frac{\phi_{skin}}{P_{skin}} + \frac{\phi_{core}}{P_{core}} \right)^{-1} \quad (4)$$

where ϕ_{skin} and ϕ_{core} are the volume fractions of skin and core, respectively.

The different layers were also heterogeneous and were individually modeled as composites. To obtain the permeability of the microlayer injection molded above the melting temperature of PA66, the skin was modeled as PA66 rods dispersed in PP ($G = 1$ in Eq. (2)) and the core as PA66 spheres dispersed in PP ($G = 2$ in Eq. (2)) using the permeability of compression molded PA66 as P_d. The results were combined in Eq. (4) with volume fractions ϕ_{skin} and ϕ_{core} taken from the micrographs as 0.3 and 0.7, respectively. The calculated value of P is included in Table 4. This approach slightly overestimated the permeability.

In the skin of the injection molded microlayer, the PA66 phase was dispersed as platelets of very high aspect ratio aligned perpendicular to the flux. Good orientation and high aspect ratio of the platelets allowed them to be represented by a series combination of PP and PA66. Assuming that the composition of the skin was the average composition, the permeability of the skin layer was calculated from Eq. (3) using the permeability of extruded and annealed PA66 for P_d. The complex morphology of the core was represented as cylindrical PA66 domains dispersed in the PP matrix (Fig. 6). The permeability of the core was obtained from Eq. (2) with G equal to unity. Any PP incorporated into the cylinders was neglected. The results were combined in Eq. (4) with the volume fractions ϕ_{skin} and ϕ_{core} taken from the micrographs as 0.3 and 0.7, respectively. The calculated permeability using the composite model is given in Table 4. The composite model that incorporated the morphology of the skin–core structure qualitatively predicted the permeability of the complex structure. The overall permeability obtained from Eq. (4) was primarily determined by the volume fraction and permeability of the least permeable constituent layer, which was the skin. Approximating the high aspect ratio PA66 platelets in the skin as continuous layers probably led to an underestimation of the permeability.

4. Conclusions

The study demonstrated that injection molding polymer microlayers produces materials with enhanced gas barrier compared to conventional polymer blends. Achieving this result requires retention of the layered structure of the dispersed phase. With PP and PA66 as the constituents, the 100 °C difference in melting points provides a broad processing window in which the PP layers melt to form the matrix whereas the PA66 layers remain in the solid state as dispersed microplatelets. Models based on the observed morphology indicate that the enhanced permeability of injection molded microlayers is provided primarily by the skin component of the skin–core structure where the elongational flow disperses the PA66 as oriented, flat platelets of high aspect ratio. Considerable curvature of PA66 platelets in the core, induced by the shear fields encountered during injection molded, severely compromises the tortuosity effect anticipated from the high aspect ratio platelets.

Acknowledgements

This research was generously supported by the National Science Foundation, Grants DMR-0080013 and DMR-9975774. Support from Modern Controls, Inc. for development of a facility for gas-transport studies at Case Western Reserve University is gratefully acknowledged.

References

[1] Weinkauf DH, Paul DR. Effects of structural order on barrier properties. In: Koros WJ, editor. Barrier properties and structures. Washington, DC: American Chemical Society, 1990. p. 60–91.
[2] Subramanian PM. Polym Engng Sci 1985;25:483–7.
[3] Subramanian PM, Mehra V. Polym Engng Sci 1987;27:663–8.
[4] Kamal MR, Garmabi H, Hozhabr S, Arghyris L. Polym Engng Sci 1995;35:41–51.
[5] Lohfink GW, Kamal MR. Polym Engng Sci 1993;33:1404–20.
[6] Lee SY, Kim SC. Polym Engng Sci 1997;37:463–75.

[7] Holsti-Miettinen RM, Perttilä KP, Seppälä JV, Heino MT. J Appl Polym Sci 1995;58:1551–60.
[8] Xanthos M, Grenci J, Dagli SS. Proc. SPE ANTEC 95. p. 3194–200.
[9] Barger MA, Shrenk WJ. Lamellar injection molding process for multiphase polymer systems. In: Stevenson JF, editor. Innovation in polymer processing molding. Cincinnati, OH: Hanser Gardner Publications, 1996.
[10] Mueller CD, Nazarenko S, Ebeling T, Schuman TL, Hiltner A, Baer E. Polym Engng Sci 1997;37:355–62.
[11] Ebeling T, Norek S, Hasan A, Hiltner A, Baer E. J Appl Polym Sci 1999;71:1461–7.
[12] Jarus D, Hiltner A, Baer E. Polym Engng Sci 2001;41:2162–71.
[13] Shur TJ, Rånby B. J Appl Polym Sci 1975;19:2143–55.
[14] Shur TJ, Rånby B. J Appl Polym Sci 1976;20:3105–19.
[15] Shur TJ, Rånby B. J Appl Polym Sci 1976;20:3121–31.
[16] Beltrame PL, Citterio C, Testa G, Seves A. J Appl Polym Sci 1999;74:1941–9.
[17] Sekelik DJ, Stepanov EV, Nazarenko S, Schiraldi D, Hiltner A, Baer E. J Polym Sci Part B: Polym Phys 1999;37:847–57.
[18] Polyakova A, Stepanov EV, Sekelik D, Schiraldi DA, Hiltner A, Baer E. J Polym Sci Part B: Polym Phys 2001;39:1911–9.
[19] Paul DR, Yampol'skii YP. Introduction and perspective. In: Paul DR, Yampol'skii YP, editors. Polymeric gas separation membranes. Boca Raton, FL: CRC Press, 1994. p. 1–81.